#### ORIGINAL RESEARCH



# Liquid penetration in hydrophobised cellulose based sheets

R. J. K. Nicasy · C. Waldner · S. J. F. Erich · O. C. G. Adan · U. Hirn · H. P. Huinink

Received: 16 January 2024 / Accepted: 26 April 2024 / Published online: 9 May 2024  $\circledcirc$  The Author(s) 2024

Abstract Controlling the liquid transport within cellulose-based materials is crucial for numerous applications, including printing, bio-assays, packaging, and cleaning. To control liquid transport and quality, post-processes such as calendering, a way of compressing and smoothen the paper using hard pressure rollers, and hydrophobisation, are commonly employed. To understand how these processes influence liquid uptake, this study uses an Ultra-Fast Imaging (UFI) NMR method to analyse moisture profiles during liquid uptake in various cellulose-based paper sheets with diverse levels of hydrophobisation and calendering. It is demonstrated that calendering decreases penetration speed and increases swelling. The reduction in penetration speed could be linked to a decrease in permeability upon calendering, as measured by the Gurley air permeance. Additionally, it is observed that hydrophobisation delayed and slowed down liquid uptake in the paper samples, and, in extreme cases, completely altered the liquid uptake phenomena. With substantial hydrophobisation, liquid penetration no longer proceeded with a well-defined liquid front but exhibited huge levels of fingering. Furthermore, is was observed that within highly hydrophobised paper, fibres were first prewetted, initiating a first swelling, before the pores between fibres could be filled. Subsequently, water could enter the pores between, allowing fibre bonds to be broken, leading to a second swelling of the paper sheet. The improved understanding will contribute to better control of the flow within cellulose-based materials, benefiting applications such as printing, packaging and microfluidics.

**Keywords** NMR · Cellulose · Liquid penetration · Darcy · Calendering · Hydrophobisation

R. J. K. Nicasy · S. J. F. Erich · O. C. G. Adan · H. P. Huinink (⋈) Applied Physics Department, Eindhoven University of Technology, P.O. Box 513, Eindhoven 5600 MB, The Netherlands e-mail: h.p.huinink@tue.nl

R. J. K. Nicasy

e-mail: r.j.k.nicasy@tue.nl

S. J. F. Erich

e-mail: bart.erich@tno.nl

O. C. G. Adan

e-mail: olaf.adan@tno.nl

C. Waldner · U. Hirn
Institute of Bioproducts and Paper Technology, TU Graz,
Inffeldgasse 23, 8010 Graz, Austria
e-mail: waldnercarina@gmail.com

U. Hirn

e-mail: ulrich.hirn@tugraz.at

C. Waldner · U. Hirn CD Laboratory for Fibre Swelling and Paper Performance, Inffeldgasse 23, 8010 Graz, Austria

S. J. F. Erich · O. C. G. Adan Organization of Applied Scientific Research, TNO, P.O. Box 49, Delft 2600 AA, The Netherlands



## Introduction

Cellulose-based materials such as paper, have experienced growing interest in the last decades in application such as packaging, driven by their renewable and biodegradable nature and the rising environmental concerns imposed by materials such as plastics (Ilyas et al. 2018; Derraik 2002). In the pursuit of minimising environmental impact and develop circular economies, efforts are made to replace existing materials with paper and other biopolymers (Dziuba et al. 2021; Babaremu et al. 2023). However, paper and biopolymers-based materials exhibit complex structures, which greatly influence the end-use properties such as printability and packaging performance. Consequently, extensive research is focused on the effects of introducing these materials for packaging systems (Tang et al. 2012; Thuppahige et al. 2022; Tayeb et al. 2020), barrier layers (Xu et al. 2020) and paper-based diagnostics (Songok and Toivakka 2016; Gong and Sinton 2017). Beyond enhancing the biodegradability of existing and new applications, research is also devoted to understanding and refining the printability of pulp and paper products (Y. Li and He 2011; Lundberg et al. 2011). This can drastically reduce the usage of harmful chemical components such as inks.

To enable fibre-based cellulosic materials, such as paper, to compete with existing applications or to enhance printability, the materials in sheet form are often modified to influence the penetration behaviour of liquids, their strength or smoothness. While certain materials, such as tissues, are specially designed to absorb water, other applications, including textiles, medical applications or food packaging require, resistance to water (Samyn 2013). Fully controlling water transport in cellulosic materials through specific liquid-surface interaction has advantages in general printing, printable electronics (Rida et al. 2009), microfluidic devices and lab-on-chip devices (Wulz et al. 2021; Böhm and Biesalski 2017; Songok and Toivakka 2016; Li et al. 2010). Therefore, multiple processes are employed to influence the penetration behaviour in the final applications (Böhm and Biesalski 2017; Li et al. 2010). Two factors that significantly influence the penetration behaviour are the porous structure and the surface chemistry of the biopolymer fibres. Calendering and sizing are two commonly used processes to adjust the porous structure or surface chemistry. In sizing, the surface chemistry of the fibres is modified to change the hydrophobicity, while calendering influences the porous structure by compressing. In sizing, a hydrophobic sizing agent is applied to the paper sample (surface sizing) or attached to the fibres (internal sizing) which hydrophobises the paper (Samyn 2013). By increasing the hydrophobicity, the paper becomes more resistant to water and moisture. The vulnerability of biopolymers and paper to wetting is a significant concern in packaging and barrier materials which can be overcome by sizing. Szlek et al. (2022) provide a detailed description of various sizing treatments to improve the hydrophobic nature of cellulose-based and other polysaccharide barriers for sustainable food packaging. Besides protection against water damage, controlled hydrophobicity can be employed to adjust the penetration speed for desired properties, and for example to define the flow path within paper-based microfluidic devices by selectively hydrophobising certain areas of the sheet (Li et al. 2010). While sizing is used to modify the hydrophobicity of the paper, as previously mentioned, calendering is used to adjust the porous structure. During calendering, paper is passed through a series of steel rollers that press the fibres together (Browne and Crotogino 2018). In some cases, these forces are accompanied by a heat treatment. Calendering increases the density of the paper, reduces surface roughness, enhances uniformity and increase paper gloss (Vernhes et al. 2009). A smoother surface primarily improves print quality, while uniformity in the paper improves workability or folding. Both outcomes contribute to improvements in the quality of the finished products.

Given that both sizing and calendering significantly influence processes such as ink or liquid penetration, swelling, and water resistance, it is crucial to improve our understanding of these processes in respect to wetting behaviour. This will lead to improvements in production speed, production cost, and quality of the paper-based materials in a variety of applications. Penetration behaviour in cellulosic material mainly depends on four processes: 1) liquid phase penetration in the capillaries (inter-fibre space), 2) surface transport along the fibres, 3) diffusion within fibres and 4) vapour phase transport. The contribution of these processes depend on the porous structure and chemical nature of the fibres which are both adjusted by processes such as calendering and sizing. While there is extensive research



on the penetration of water and aqueous liquids into materials such as paper (Oliver et al. 1994), cellulosic materials (Wu et al. 2009), and random fibres network (Hodgson and Berg 1988; Vallabh et al. 2011), the research on effects such as calendering and hydrophobisation on that penetration is significantly less. However, several studies address the effects of sizing and calendering on phenomena such as print dot spreading (Waldner et al. 2023; Kannangara and Shen 2008), wettability (M. von Bahr et al. 2004; Modaressi and Garnier 2002), mechanical strength (Korpela et al. 2021), changes in local roughness (Xie et al. 2008), ink setting behaviour (Resch et al. 2010) and printability (Wulz et al. 2021). Although, these studies offer information about the effect on parameters such as printability, gloss, and water resistance, they provide limited insight into the physics and exact penetration behaviour. Most of these studies use techniques such as ultrasonic response to liquid penetration (Waldner et al. 2022), drop adsorption (Waldner et al.) or automatic scanning absorptometer (Y. Xu and Enomae 2014; Kuijpers et al. 2018), all of which can give a good idea about the effects of calendering and sizing on the penetration speed by measuring the total absorbed liquid as a function of time. Highspeed cameras have also been used to study effects of sizing and calendering on droplet shape (Kannangara and Shen 2008), fibre density and porous structures (Browne and Crotogino 2018). However, all these techniques are unable to provide information about the local moisture content within the fibres matrix through time. Consequently, it becomes challenging to present a full picture of the penetration process and the effect and contribution of different transport processes such as film flow, swelling, vapour transport and transport within fibres. Some attempts are made to incorporate the surface energies within the penetration process (Waldner and Hirn 2023). However, the use of models becomes very difficult because the contributions of the varying processes remain unclear.

To enhance our understanding about effects such as calendering and hydrophobisation on liquid penetration and provide validation for existing models, an experimental study providing moisture distributions on relevant time scales is necessary. In a previous study, we showed that an Ultra Fast Imaging (UFI) NMR method was able to measure the moisture distribution within paper samples with a temporal resolution of  $10~{\rm ms}$  and spatial resolution of  $18~{\rm \mu m}$ 

(Nicasy et al. 2024). These profiles enabled information to be extracted about moisture density, swelling and structural deformation during and after liquid penetration. The study showed that within hydrophilic, lightly calendered paper, the penetration process could be divided into three phases, liquid uptake, swelling and release of trapped air. While this previous study improved our knowledge about the liquid uptake in hydrophilic paper, it did not investigate the effect of calendering and hydrophobisation.

The aim of this current study is to provide spatial moisture distributions during the penetration of a water-based solutions within a diverse range of calendered and hydrophobised paper samples. The resulting moisture profiles offer valuable insights into the liquid penetration behaviour, swelling kinetics and structural changes within the paper samples during and after penetration. With these findings we can deepen our understanding of the physics governing liquid penetration within paper and the contribution and importance of varying processes such as calendering and hydrophobisation to target specific end product properties.

#### Materials and methods

Substrates

Various paper sheets with differing degrees of calendering and hydrophobisation were examined. The papers were taken from a study performed by Waldner et al. (Waldner and Hirn 2023). Table 1 summarises the most important parameters and characteristics. The sheets are made from an industrially produced uncoated paper composed of cellulose pulp (bleached eucalyptus kraft) and calcium carbonate filler (scalenohedral, precipitated calcium carbonate, filler content 21.25%). The surface energy of the paper was modified using chemical vapour deposition. The hydrophobisation agent was hexamethyldisilazene (HMDS, from Carl Roth, 98%). Four hydrophobisation levels were obtained by applying either 0 (H00), 10 (H10), 20 (H20), 40 mL (H40) of HDMS per 10 A4 sheets. After hydrophobisation, the papers were calendered using a force of 0 (C00), 15 (C15), 30 (C30) or 60 (C60) kN, which resulted in a line load of 0, 71, 143, and 286 kN m<sup>-1</sup>. The Gurley method (ISO 5636-5) is used to obtain a first approximation



5530 Cellulose (2024) 31:5527–5544

**Table 1** Physical properties of the paper samples, data from Waldner et al. (Waldner and Hirn 2023)

| Paper       | Thickness [µm]  | Apparent<br>density [g<br>cm <sup>-3</sup> ] | Mean pore<br>diameter<br>[µm] | Water contact angle $\theta$ [°] | Gurley air permeance $\kappa_G$ [ $\mu$ m Pa <sup>-1</sup> S <sup>-1</sup> ] |
|-------------|-----------------|----------------------------------------------|-------------------------------|----------------------------------|------------------------------------------------------------------------------|
| Reference   |                 |                                              |                               | '                                |                                                                              |
| C00H00      | $132.4 \pm 1.9$ | 0.68                                         | 2.80                          | 38.0                             | $11.5 \pm 0.2$                                                               |
| Calendering |                 |                                              |                               |                                  |                                                                              |
| C15H00      | $100.0\pm1.2$   | 0.90                                         | 2.16                          | 39.0                             | $5.0 \pm 0.1$                                                                |
| C30H00      | $94.9 \pm 2.6$  | 0.94                                         | 1.89                          | 41.0                             | $3.0 \pm 0.1$                                                                |
| C60H00      | $92.3 \pm 2.1$  | 0.97                                         | 1.51                          | 46.9                             | $2.1 \pm 0.1$                                                                |
| Hydrophobis | sation          |                                              |                               |                                  |                                                                              |
| C00H10      | $134.3 \pm 2.5$ | 0.67                                         | 2.80                          | 82.8                             | $11.9 \pm 0.3$                                                               |
| C00H20      | $132.4 \pm 1.7$ | 0.68                                         | 2.80                          | 104.5                            | $11.6 \pm 0.5$                                                               |
| C00H40      | $132.0 \pm 2.8$ | 0.68                                         | 2.80                          | 114.6                            | $11.7 \pm 0.4$                                                               |
|             |                 |                                              |                               |                                  |                                                                              |

about the papers permeability. The Gurley air permeance  $\kappa_G[\mu m. Pa^{-1}. S^{-1}]$  gives the volumetric air flow, averaged over the measurement area and pressure. For a detailed description of the paper samples, Gurley air permeance measurements and the preparation process, readers are referred to the original paper by Waldner et al. (Waldner and Hirn 2023).

## Test liquids

For the liquid uptake experiments, a Clariscan<sup>TM</sup>water solution was used. The solution consists of demineralised water type 1 and 0.04 mol L<sup>-1</sup> Clariscan<sup>TM</sup>. The Clariscan<sup>TM</sup> was added to control the NMR relaxation time and increase the signal-tonoise ratio as explained by Nicasy et al. (Nicasy et al. 2023). The Clariscan<sup>TM</sup> comes from GE healthcare AS and was provided by the Máxima Medisch Centrum. The Clariscan<sup>TM</sup> comes in a water like solution with a concentration of 279.3 mg mL<sup>-1</sup> (0.5 mol/l), a viscosity of 3.0 mPa.s, a pH between 6.5 and 8 and a density of 1.349 g mL<sup>-1</sup>. The viscosity and surface tension of the Clariscan<sup>TM</sup>-water solution were measured using an Anton Paar MCR302 rheometer (20 °C) and the pendant drop method to be 1.09 mPa s and 67.3 mN m<sup>-1</sup>, respectively

# Nuclear magnetic resonance

Nuclear magnetic resonance (NMR) measurements were used to follow the liquid distribution during uptake. The measurements were performed on a home-built GARField NMR with a home build

acquisition system. The main magnetic field strength  $(B_0[T])$  was 1.47 T, and the static gradient  $(G [T m^{-1}])$  was 41.5 T m<sup>-1</sup>. The signal was recorded with a radio frequency (RF) coil having a diameter of 4 mm. Subsequent data analysis was carried out using MATLAB.

Liquid profiles were measured using an Ultra Fast Imaging Nuclear Magnetic Resonance (UFI-NMR) method, described in earlier work (Nicasy et al. 2023). This technique uses an adaptation of the OW-sequence with two additional elements, namely, a contrast agent (Clariscan<sup>TM</sup>) to optimise signal intensity and the summation of multiple echoes to ensure a rapid decrease in signal-to-noise ratio. The specific pulse sequence is given by:  $90_x^{\circ} - \tau - \left[90_y^{\circ} - \tau - (echo) - \tau - 90_{-y}^{\circ} - \tau - (-echo) - \tau\right]_y$ , where N = 16 represents the number of repetitions. In this study, the echo time  $(t_e = 2\tau)$  was set to 50 µs with a window width of 40 µs. The time between two pulsed experiments and therefore moisture profiles was set to 10 ms. The setup allowed for the storage of 80 profiles before data transfer was required, leading to a measurement period of 0.8 s  $(80 \times 10 \text{ ms})$  followed by a 6 – 8 s dead-time. Practically, this implies that in this case profiles can be measured in the following timestamp: 0 s - 0.8 s, 6 s - 6.8 s, 12 s—12.6 s etcetera. The time between these periods depends on the dead time and varies between 6 - 8 s. For more information about this sequence we refer to earlier work (Nicasy et al. 2024). The pulse length was set to 1 µs and kept constant for all experiments. This relatively short



pulse length setting was chosen to achieve the maximum field-of-view, which was around 400  $\mu m$ .

With these settings, moisture profiles were acquired with a spatial resolution of 14.5 µm and a temporal resolution of 10 ms. A previous study demonstrated how the UFI-method is able to visualise <sup>1</sup>H-atoms of the liquid solution but is unable to visualise <sup>1</sup>H-atoms from other sources, such as freezing and non-freezing bound water, cellulose or fillers due to their short NMR-relaxation times (Nicasy et al. 2024). Figure 1 shows a schematic representation of the experimental setup, including a corresponding moisture profile as measured by the UFI-method: shown are the droplet and paper together with the droplet-paper interface (yellow dashed line) and liquid front (black dashed line). The moisture profile (orange line), droplet-paper interface and liquid front are also visible on the UFI moisture profile, shown right in Fig. 1. In the setup, the sample can be seen, which consists of a paper glued on top of a glass plate using double sided tape. The sample was placed within a glass container that could be closed by a cork to prevent evaporation. The droplets were jetted from a height of 2 cm using BRAND® PD-Tips II with a volume of 0.1 ml. The final droplet had a volume around 8 µl. The RF-coil seen below the sample was used to measure the moisture profiles.

## Effect of calendering

To study the influence of calendering, liquid penetration experiments were performed using a Clariscan-water mixture on a reference paper (C00H00) and several non-hydrophobised calendered papers (C15H00, C30H00 and C60H00). The first part of this section will concentrate on a comparison between the moisture distributions during penetration of the reference paper and a heavily calendered paper only, in order to highlight the major changes, thus providing insights into swelling, liquid penetration speed and moisture content during penetration. Later, these three parameters will be discussed in more detail. Finally, the correlation between the liquid front and swelling will be discussed.

Figure 2 shows the liquid profiles measured during the penetration of a Clariscan-water solution within a lightly-calendered paper (C00H00) and a high-calendered paper (C60H00). For the purpose of this section, the profiles for the samples C15H00 and C30H00 are not shown but can be found in appendix 1. The profiles represent the droplet area, paper sample and double-sided tape. In both measurements, at t=0 s, the droplet is situated at x<0 µm and has a signal intensity of 1 representing 100% saturation since the droplet consists entirely of liquid. At t<0, before the droplet hits the paper sheet, the paper is dry, and

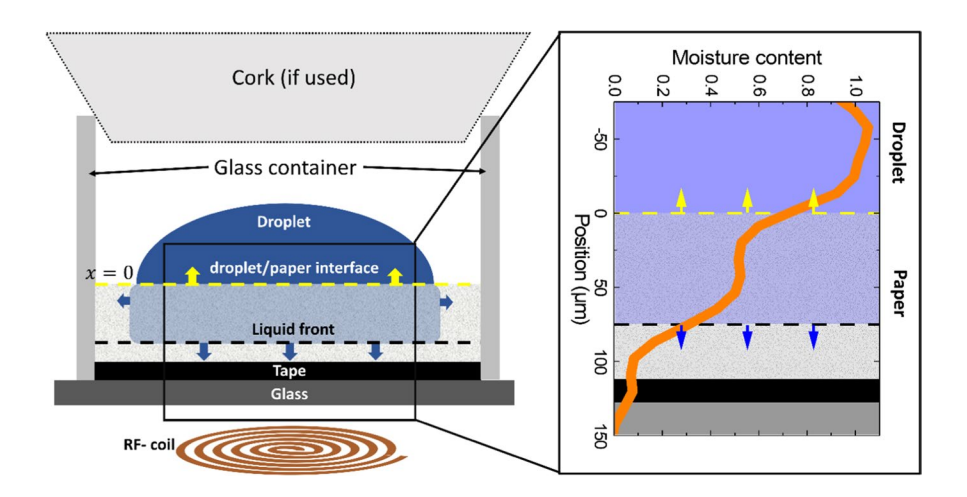


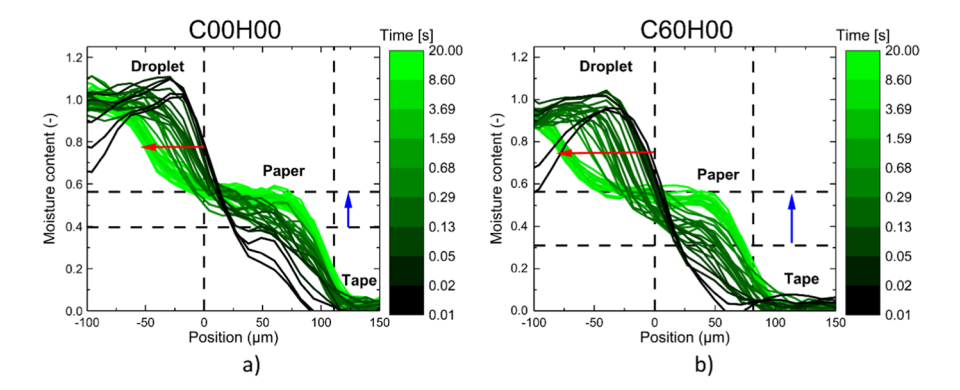
Fig. 1 Schematic representation of the experimental setup. Shown is a droplet on top of a paper sample. The sample is glued with tape (black) on top of a glass plate (dark grey) and is surrounded by a glass container, which can be closed by a cork in case evaporation should be prevented. Below the sam-

ple is the RF-coil, which is used to measure the NMR-signal. Next to the schematic setup, the corresponding moisture profile as measured by the NMR is given (orange line). In both images, the liquid front is marked with a black dashed line and the droplet-paper interface is marked with a yellow dashed line



5532

Fig. 2 Liquid profiles measured during the penetration of a Clariscanwater solution within a) C00H00, a reference paper, and b) C60H00, a paper. A green colour map is used to mark the time at which the profile is measured



no moisture is observed in the paper sheet. These zero signal profiles are not shown on these images.

In Fig. 2a, the paper has a thickness of approximately 115  $\mu$ m and is located between 0 and 115  $\mu$ m. In the case of the highly calendered paper, shown in Fig. 2b, the paper thickness reduces to 80  $\mu$ m which is a direct consequence of the calendering process. The decrease in paper thickness upon calendering was also shown in Table 1.

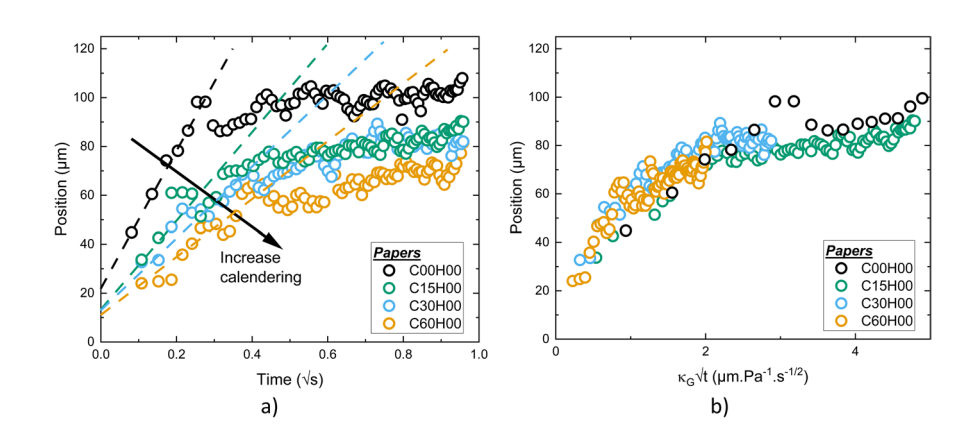
For both measurements, swelling was observed as a movement of the droplet-paper interface, indicated by a red arrow. Consistent with prior research (Nicasy et al. 2024), during swelling a moisture increase was observed within the paper samples, as indicated by a blue arrow. The initial moisture content at the start of swelling (marked with dashed line) was taken from the moisture profile just after the liquid front reached the end of the paper,  $t=80~{\rm ms}$  (C00H00) and  $t=130~{\rm ms}$  (C60H00). In that study, this moisture increase was attributed to two phenomena: swelling, which increased the internal porosity, and the removal of air which was entrapped by the liquid front.

Liquid penetration

The profiles provide information about the influence of calendering on penetration behaviour. It was evident from the profiles that calendering affected the penetration speed of the water-Clariscan mixture, as observed by the slower movement of the profiles inside the C60H00 paper. Liquid front positions were extracted over time at a moisture content of 0.2 (-), where a saturation of 1 corresponds with a fully saturated region. It is important to note that ideally, liquid front positions are extracted at half the maximum moisture content. This becomes more challenging in papers with higher levels of calendering as the moisture content varies significantly through time, making the front positions of highly calendered papers less accurate.

Figure 3a shows the liquid front position as a function of the square root of time for papers with varying degrees of calendering. The penetration data were analysed until the water reached the bottom of the paper which varied between 0.2—0.4 s

Fig. 3 Liquid front positions as a function of a) t and b)  $\kappa_G \sqrt{t}$ , for the penetration of a Clariscanwater solution within a C00H00 reference paper (black) and higher C15H00 (green), C30H00 (blue) and C60H00 (orange) paper. The liquid front positions are taken from the profiles shown in Fig. 2 at a moisture content of 0.2 (-)





depending on the level of calendering. Thereafter, the position slowly increased due to an artefact coming from the further increase in moisture content. In all cases, data reveal a square root of time behaviour for the first part of the penetration as predicted by Darcy, see dotted lines in \\* MERGEFORMAT Fig. 3a (Huinink 2016; Darcy 1856). The data illustrate how calendering decreased penetration speed. Since both papers were chemically similar (unsized), changes within the porous structure, such as tortuosity, should be responsible for the decrease in penetration speed. This is explained by models such as Darcy and Washburn, were the fluid front position scales with pore radius. In these models, capillary pressure is taken as the driving force and the permeability is a value which represent the porous media properties. While the capillary pressure scales with 1/r, the permeability scales with  $r^2$  (Huinink 2016). Therefore, the fluid front scales linearly with the pore radius. A better approximation on the influence of the porous structure can be achieved using the Gurley air permeance  $\kappa_G$ , in Table 1. Although  $\kappa_G$  represents the air flow through a specific paper sheet rather than a real permeability, both can be related to each other using paper properties (Shallhorn and Gurnagul 2009). Because the paper properties of all sample are similar, a rescaling with the Gurley air permeance is justified and can be used as a first approximation to account for the permeability. When rescaling the data using Darcy's Law and the Gurley Air permeance  $(\kappa_G)$  Table 1) with  $\kappa_G \sqrt{t} [\mu m \text{ Pa}^{-1} \text{ s}^{-1/2}]$ , the data converge relatively well onto one master curve Fig. 3b), suggesting that the Gurley Air permeance is a suitable measure for determining changes in the pore structure of the paper such as permeability or tortuosity for liquid penetration.

## Swelling

The profiles also provide insight into the swelling behaviour of the papers. By examining the droplet membrane interface, the paper thickness can be followed over time. At t=0 s, the droplet-membrane interface was located at x=0 µm. However, paper swelling resulted in a movement of the droplet-membrane interface (indicated by a red arrow in Fig. 2). By tracking the interface at a moisture content of 0.75, the paper thickness  $d_t$  at time t was determined. Swelling S(%) was calculated using the formula,

 $S(\%) = 100(d_t - d_0)/d_0$ , where  $d_0$  represents the initial paper thickness at  $t\!=\!0$  s. Figure 4 illustrates the swelling in percent as a function of time for the C00H00 reference paper (black) and the C60H00 calendered paper (orange). For clarity, only the reference paper and highly calendered paper are shown, while data for other calendered papers can be found in appendix 1. It was observed that the C60H00 paper swelled more than the reference C00H00 paper.

The process of swelling arises from internal stresses and water diffusion within the fibres. While models exist for this stress-diffusion coupling in fibrelike porous media, they often require numerical solutions due to their complexity (Seidlhofer et al. 2022; Blanco et al. 2013). In this study, a simpler model is used, which links paper swelling S(%) to a rate constant  $k(s^{-1})$  via  $S = S_{max}(1 - e^{-kt})$ . Here,  $S_{max}$  represents the equilibrium swelling degree (maximum possible swelling), and k a rate constant which can be associated with diffusion in the fibres, relaxation of the fibres, or a combination of both (Benmessaoud et al. 2020; Yavari and Azizian 2022; Zhang et al. 2020). k can also be related to a time  $t_d = 1/k$ , where  $t_d$  is the time required for the paper to reach 0.63 of its maximum swelling. The fit for both papers is given in Fig. 4, yielding values of  $k = 2.06 \pm 0.1s^{-1}$ and  $S_{max} = 45 \pm 0.4\%$  for C00H00 and values of  $k = 1.92 \pm 0.1 \, s^{-1}$  and  $S_{max} = 87 \pm 0.5 \%$  for C60H00. The similarity in rate constants suggest a comparable swelling mechanism. Because the fibres of both

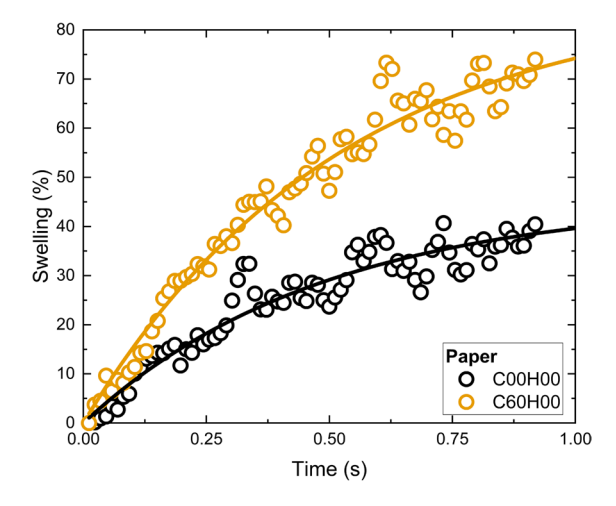


**Fig. 4** Swelling as a function of time for C00H00 (black) and C60H00 (orange). The lines corresponding to a fit based on a swelling model given by:  $S = S_{\text{max}}(1 - e^{-kt})$ 



papers are identical, diffusion in the fibres should be comparable. On the other hand, the more compressed calendered paper should have an increased relaxation behaviour due to the higher fibre density. This lets to the conclusion that at this time period, diffusion in the fibres drives swelling. The higher swelling of the highly calendered paper compared to lightly calendered paper can be attributed to differences in fibre density between the two papers..

Considering that k is related to the diffusion in the fibre walls, a first estimation of the diffusion constant can be made. Using Fickian diffusion, the diffusion constant (D) can be calculated by  $D = l_d^2/2t_d$ . Taking  $l_d$ , as the typical thickness of the fibre wall (2–5  $\mu$ m), a diffusion constant D=4.2 • 10<sup>-11</sup> m²/s is obtained, which aligns reasonable well with values for radial diffusion in in wood fibres as found in literature (Arends et al. 2018; Saft and Kaliske 2013).

This aligns with the observation that initially pores are saturated with water before swelling occurs, meaning that water penetrates from the radial direction into the fibres. This water penetration initiates paper swelling. The maximum swelling is determined by the fibre density of the paper sheets, which is influence by the degree of calendaring.

## Moisture content

Finally, the profiles also provide information about the moisture content, indirectly offering insight into the paper structure. In a previous study, we demonstrated that, for the reference paper (C00H00), during swelling, the paper's porosity increased, leading to a rise in the moisture content (Nicasy et al. 2024). A similar moisture content increase was also observed within the highly calendered paper as indicated by blue arrows in Fig. 2. Figure 5 shows the moisture content as a function of time for the reference paper as taken from Nicasy et al. (Nicasy et al. 2024), represented by the black data points and as measured for the highly calendered paper C60H00, orange data points. The moisture content was integrated between  $38 - 50 \mu m$  in the reference paper and between 40 – 52 µm for the C60H00 paper. For the reference paper, the moisture content increased from 0.4 to 0.55. However, for the highly calendered paper, the moisture content increased from 0.3 to 0.55. This observation led to two main findings. First, the calendered paper has a lower initial porosity, resulting

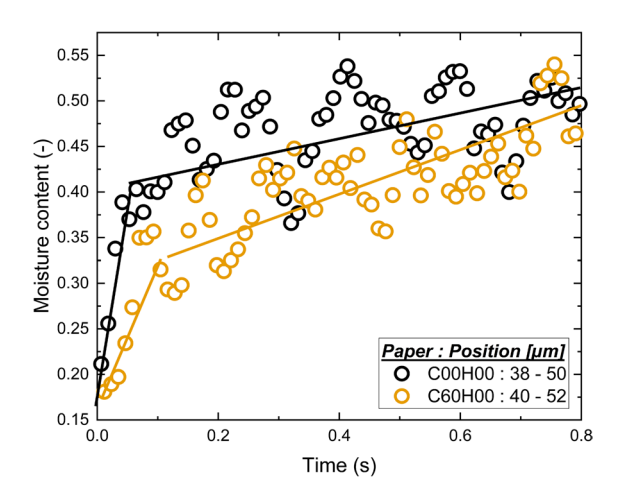


Fig. 5 Moisture content as a function of time in a C00H00 (black) and C60H00 (orange) paper during the penetration of a Clariscan-water solution. The moisture content was determined between 38 and 50  $\mu$ m in the C00H00 paper and between 40 – 52  $\mu$ m for the C60H00 paper

in a lower moisture content at the start. Second, after swelling, both papers had similar moisture contents, indicating that the effect of calendering disappeared after swelling, and this again supports the topological nature of compression and its effect on tortuosity only.

# Liquid front vs swelling

In the final part of this section, the relationship between liquid front and swelling will be discussed. Figure 6 shows the liquid front position as a function of swelling for the C00H00 reference paper (filled circles) and the C60H00 calendered paper (open squares). A colour code is used to mark the time of the data points. In a previous study it was shown that for a lightly calendered hydrophilic paper such as the reference paper, liquid first penetrated the entire paper before swelling occurred, see purple arrow in Fig. 6 (Nicasy et al. 2024). Differently, for a calendered paper, where penetration was significantly slowed down (Fig. 3) swelling already occurred during penetration, as seen in Fig. 6 (black arrow).

The relationship between the liquid front and swelling provides valuable information for theoretical models and simulations. The data show that for our reference paper, (hydrophilic, pore radius > 2.8 µm, and initial porosity > 0.4), theoretical models and



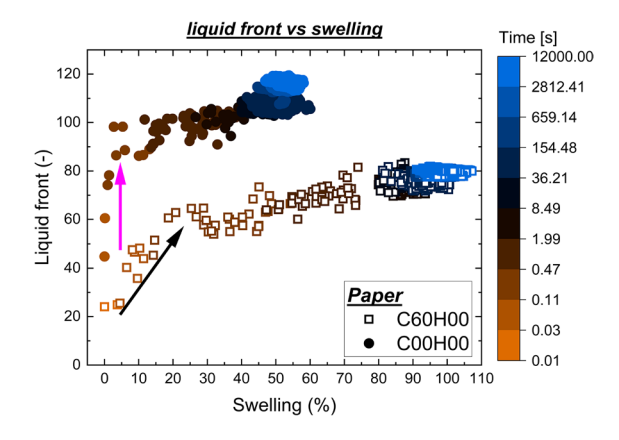


**Fig. 6** Liquid front as a function of paper swelling for the C00H00 reference paper (filled circles) and for the C60H00 calendered paper (open squares). A colour code is used to mark the time of the measurement

simulation for liquid penetration can be simplified by neglecting swelling. However, for higher calendering, which results in papers with lower pore radii and lower porosities, swelling can significantly influence the penetration process and cannot be neglected. In these particular case, incorporating swelling into the model is essential, which has been the focus of several studies (Masoodi and Pillai 2010; Chang and Kim 2020).

## Effect of hydrophobisation

To study the effect of hydrophobisation on liquid transport, penetration experiments were conducted on four papers with varying levels of hydrophobisation (C00H00, C00H10, C00H20 and C00H40), as listed in Table 1. Figure 7 displays the liquid profiles obtained during penetration of a Clariscan-water mixture within C00H10 and C00H40. Due to the similarity between the profiles of C00H20 and C00H10,

only the profiles for the C00H10 paper are shown, while those of C00H20 can be found in appendix 2. The liquid profiles for the C00H00 reference paper are shown in Fig. 2a. In these figures, a green scale is used to indicate the time of measurement.

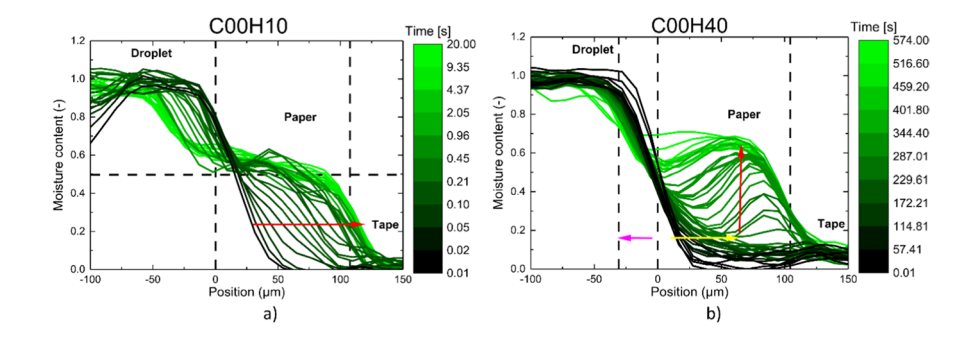
The liquid profiles revealed that papers with less hydrophobisation, such as C00H10 (Fig. 7a) and C00H20 (appendix 2 Fig. 15), exhibit similar penetration behaviour to the hydrophilic paper (Fig. 2a), showing comparable moisture profiles. Within these papers, the liquid still penetrated with a well-defined liquid front. The main influence of hydrophobising within these papers was a decrease in penetration speed. However, for higher levels of hydrophobising, as found in the C00H40 paper, the penetration behaviour completely changed, as illustrated in Fig. 7b. In this paper, the liquid did not penetrate with a well-defined liquid front but shows two distinct phases.

During the first phase, the liquid barely penetrates the paper. This is evident in the liquid profiles of Fig. 7b, where until 114 s, the liquid profiles remain relatively stationary. Only a small amount of liquid was able to penetrate within the pores of the paper sample, as indicated by a yellow arrow. After a certain moment, a second phase starts around 160 s, where the moisture content within the pore space rapidly increases (red arrow). The highly hydrophobised paper, having a completely different penetration behaviour, will be discussed in more detail in Section 4.3. But first, in Section 4.1, we will take a closer look at the moisture content within the paper and the relationship between moisture content and swelling for all different papers.

## Moisture content

To investigate the effect of hydrophobising on moisture uptake, the moisture content within the papers

Fig. 7 Liquid profiles measured during the penetration of a Clariscanwater solution within a) C00H10 and b) C00H40 paper. A green scale is used to identify the time at which the profile is measured





5536 Cellulose (2024) 31:5527–5544

was monitored over time. Figure 8a shows the moisture content as a function of time for the penetration of a Clariscan-water solution within papers with four levels of hydrophobisation: C00H00 (black), C00H10 (orange), C00H20 (blue) and C00H40 (green). The moisture content was extracted from the moisture profiles between 38  $\mu$ m and 60  $\mu$ m for the C00H00 paper and between 28  $\mu$ m and 62  $\mu$ m for the other papers. In this figure, time is plotted logarithmically. Based on these data, the liquid uptake could be divided into three main regions: 1) a delay time, in which moisture penetration is remarkably slow, only observed in hydrophobised papers, 2) a rapid moisture increase and 3) a slower moisture increase at the end.

The data indicates that hydrophobisation significantly decreased and delayed moisture uptake within a paper sheet. To acquire a first approximation of the moisture uptake rate, a linear fit is used around the point of highest moisture uptake rate. The slope of these fits are used for the moisture uptake rate. The fits were determined between 0.01 - 0.05 s (C00H00), 0.03 - 0.14 s (C00H10), 1.6 - 2.6 s (C00H20), and 290 - 330 s (C00H40). from the point when the wetting delay was over until the paper moisture level stabilised. Figure 8b shows the observed delay times for all papers in orange columns and the determined moisture uptake rates by grey columns.

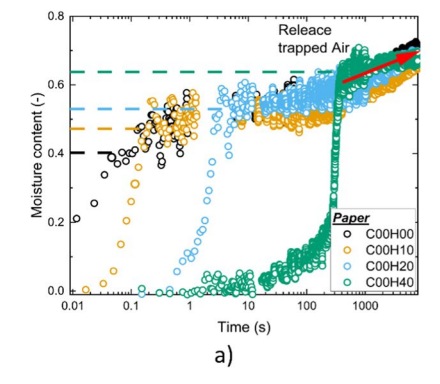
The delay time scaled almost logarithmically with hydrophobisation, doubling the hydrophobising agent concentration delayed penetration by one or more orders of magnitude, as shown in Fig. 8b by orange columns. During this delay time, moisture slowly penetrated within the paper sample, most markedly for the highly hydrophobised C00H40 paper.

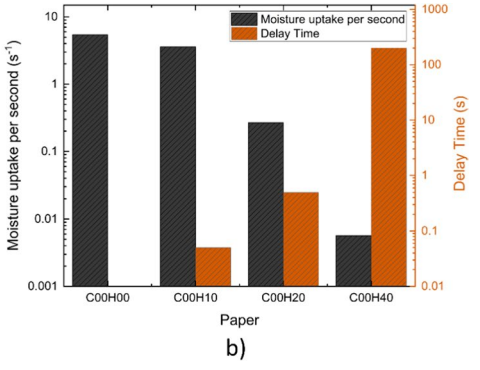
After this delay time, the moisture content rapidly increased, and the pore space was filled with water. In

the data of the C00H00, C00H10 and C00H20 papers, the sudden increase in moisture content corresponded with the movement of the liquid front through the paper sample. However, within the C00H40 paper, liquid penetration occurred differently, without a liquid front. Therefore, the sudden increase did not correspond to a liquid front but to a rapid filling of the pore space, as observed within the profiles in Fig. 7b. Therefore, it can be concluded that from a certain level of hydrophobisation, liquid penetration transitions from a liquid front towards a non-liquid front like behaviour. The particular behaviour of these systems and the sudden increase in explained in more detail in Section 4.3.

Another observation, made from Fig. 8a, was that after filling of the pore space, the moisture content became larger with increased levels of hydrophobising agent, as indicated by dotted lines. In a previous study, it was shown that for a C00H00 reference paper, the moisture content after filling first increased to 0.4 due to the movement of a liquid front (Nicasy et al. 2024). Thereafter, other effects, such as swelling and air removal further increased the moisture content towards 0.75. The phenomena of air removal was proven in earlier research, where NMR relaxation measurements showed that air was trapped during liquid front movement (Nicasy et al. 2024). Thereafter, the air slowly diffused out of the system through the top of the paper sample. Because the saturation after filling of the pore space increased with higher levels of hydrophobisation, it was believed that by decreasing the penetration speed, the paper was already able to increase its porosity due to swelling, or less air was entrapped during penetration. Since, for the lightly hydrophobised papers (C00H00, C00H10 and C00H20), the moisture increase on later timescales

Fig. 8 a) Moisture content as a function of time for penetration experiment performed with a Clariscanwater solution on varying sized papers: C00H00 (black), C00H10 (orange), C00H20 (blue) and C00H40 (green) b) observed delay times for all papers (orange columns) and the determined moisture uptake rates (grey columns)







was quite similar as shown by the red arrow, the release of trapped air can be assumed to be quite similar in all cases. Therefore, the reason for a higher moisture content after front penetration was linked to paper swelling during penetration.

For the highly hydrophobised paper, the need for release of trapped air disappeared, and the moisture content directly is seen to increase directly towards the highest level of 0.75, green data points in Fig. 8b. Therefore, in highly hydrophobised papers, the paper already swelled before penetration and the distinct penetration behaviour entrapped less air.

## Swelling vs moisture content

Figure 9 illustrates the moisture content as a function of swelling to investigate the penetration behaviour in more detail. In earlier research, it was found that for a reference paper (C00H00, filled squares) swelling occurred after liquid front penetration (Nicasy et al. 2024). Slightly hydrophobised papers, C00H10 (open circles) and C00H20 (filled triangles), exhibited similar behaviour as seen in Fig. 9. However, for the highly hydrophobised paper, C00H40 (open triangles) swelling took place before moisture appeared within the pores of the paper sample. Since swelling of paper sheets can only occur in the presence of moisture, this indicates that water must be present within the

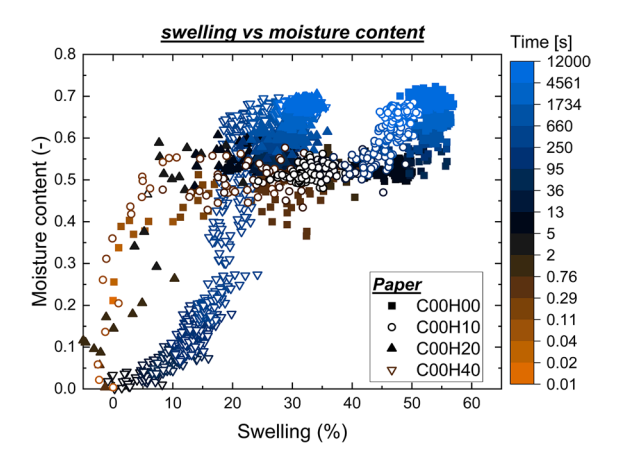


**Fig. 9** Moisture content as a function of swelling for the penetration of a Clariscan-water solution within four papers with varying levels of hydrophobisation: C00H10 (filled squares), C00H10 (open circles), C00H20 (filled triangles) and C00H40 (open triangles). A colour code is used to mark the time of the measurement

fibres before water can fill the pore space between the fibres, indicating a different wetting mechanism then for hydrophilic paper. Where for hydrophilic paper, liquid can directly penetrate due to capillary forces, in hydrophobised paper, fibres first need to be wetted before liquid uptake can take place.

This also suggests a change in the surface of the pore space which also cause swelling. Therefore, water must for sure be present along the fibres. If water were only present within the fibres, the pore spaces would remain unchanged, preventing water from entering the paper samples. The next section is devoted to understanding the different mechanism of wetting, such as wetting delay, moisture vapour diffusion, swelling, and fingering observed in highly hydrophobised papers.

# Highly hydrophobised papers

Given the distinctive penetration mechanism of the highly hydrophobised C00H40 paper, a dedicated section is devoted to supporting the understanding of the penetration within highly hydrophobised papers.

Figure 10 presents a graph depicting swelling and moisture content as a function of time for hydrophobised C00H40 paper. Based on the moisture uptake, penetration could be divided into two regimes: a slow almost linear moisture uptake and a second, faster uptake. This slow and fast uptake was also observed within the profiles in Fig. 7b. Another observation was that immediately after the paper came into contact with the droplet, the paper started to swell

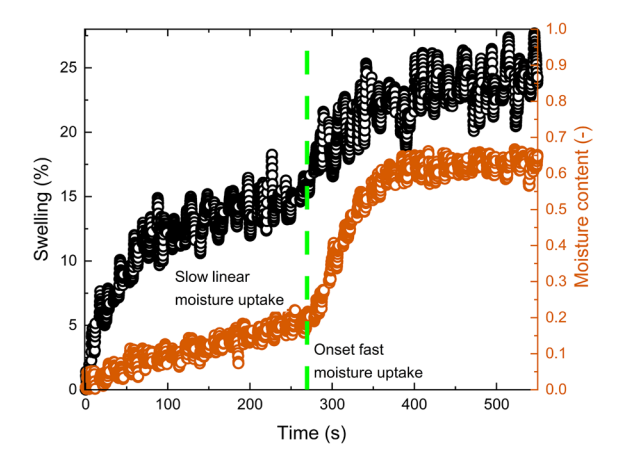


**Fig. 10** Swelling (black) and moisture content (orange) as a function of time for the penetration of a Clariscan-water solution within a highly sized C00H40 paper



5538

even when there was almost no moisture within the paper pores. This swelling continued until the paper swelled by 12.5% in thickness after which the swelling rate decreased. Furthermore, it was observed that the onset of fast moisture uptake triggered another swelling stage. Therefore, water within the pores is required to swell the paper sheets completely. This indicates that there are two swelling mechanisms: first a swelling caused by moisture uptake of the fibres and swelling caused by moisture between the fibres, probably loosening the bonding between fibres.

The peculiar behaviour of the moisture profiles in Fig. 7b and the two-phase moisture uptake can be explained by fingering. To illustrate this behaviour, pictures from the top of the C00H40 paper during penetration were captured and are shown in Fig. 11. At the start of the penetration, the droplet was clearly visible, and the paper appeared completely white. Over time, darker spots began to emerge, corresponding to saturated areas within the paper sample. The darkening is due to a change in refractive index when the paper becomes wet, making it transparent and less white as explained in other research (Murali et al. 2021). The onset of the darker spots could be related to the onset of the fast moisture uptake around 270 s after initial liquid contact, as seen in Fig. 10. Furthermore, these spots were observed to expand gradually over time. A typical spot is marked by a red arrow in Fig. 11. This illustrates that wet zones act as nucleation zones, attracting more water until the paper was fully wet and completely transparent. This mechanism of pore space filling clarifies why no liquid fronts were observed in highly sized paper in Fig. 7b.

For a better understanding of the filling mechanism in highly hydrophobised paper, a schematic representation is given in Fig. 12. The mechanism can be split into three phases.

In phase 1, a delay with very slow increasing moisture content was observed. This was attributed to the paper's hydrophobic nature, making it challenging for water to enter the pore spaces. During this slow uptake, water attempts to find a path on the fibres which is probably a combination of film flow along the fibres, gas vapour transport and flow within the fibres. During and after this transport, within a 2nd phase, water is present within the fibres which was observed by a first swelling of the paper in Fig. 10 even though no moisture was observed within the pore spaces. This swelling is attributed to an increase in fibre volume when they absorb water, see Section 3.2. After swelling, water was observed to enter the pore space (Fig. 9), therefore, fibres first need to be wetted before water can enter the pore space. A similar observation was made by Akinli-Koçak (Akinli-Kogak 1997), which showed that sorption along the interfibre pores is delayed by a wetting delay and that water first absorbed into the fibre walls before interfibre sorption occurs. This fibre wetting reduces the hydrophobicity of the surface, enabling water to enter a fully wetted pore space. The reduction in hydrophobicity (contact angle) can be linked to various phenomena such as swelling, and water vapour transport. These processes are time dependent and will therefore contribute to the dynamic character of the imbibition process.

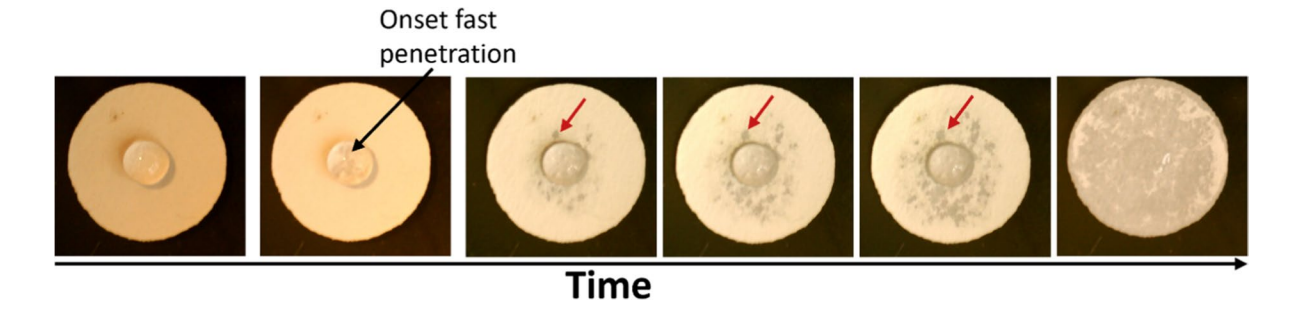


Fig. 11 Top images of the C00H40 highly sized paper during the penetration of a Clariscan-water solution. The darker spots correspond to areas which are fully saturated which make the paper more transparent



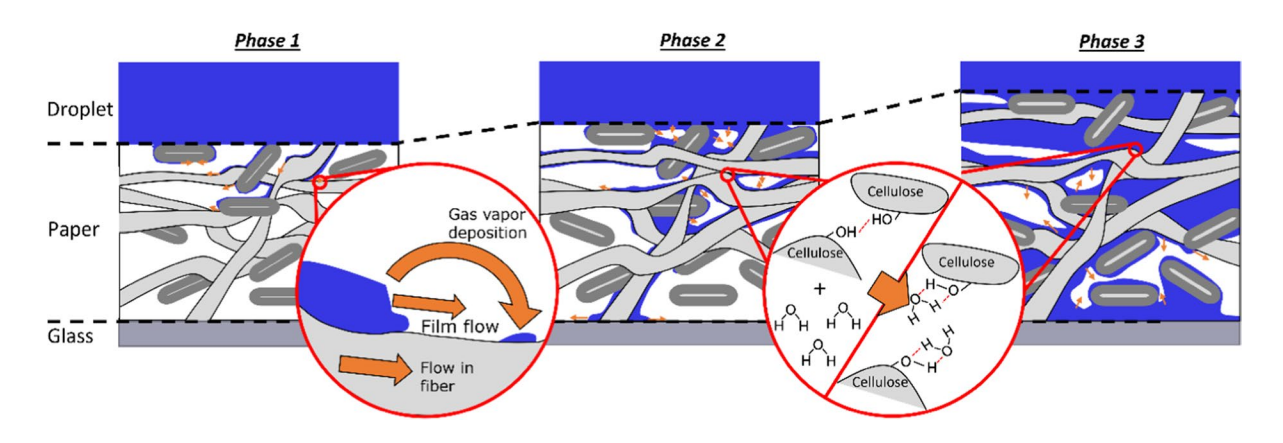


Fig. 12 Schematic representation of the liquid penetration within highly hydrophobised paper

Swelling increases the surface area of the fibres and also increases the amount of water in the fibre wall. The increased water content is raising the polar surface energy of the fibre surface and thus increases the wetting of the water drop (Waldner and Hirn 2023). There are also some suggestions that water diffusion into the fibres lowers the glass transition temperature of the amorphous cellulose in the surface, thereby allowing polar hydroxyl groups to rotate outwards, leading to a reduction of the contact angle ahead of the liquid front (Akinli-Kogak 1997).

The change in contact angle is also influenced by sorption of water molecules from the vapour phase on to the fibre wall ahead of the liquid front. The high water concentration in the vapour phase close to the liquid surface result in a diffusion of water in the vapour phase into the paper sample. The water can then condense back onto the fibres, thereby lowering the contact angle and inducing water penetration. The transport of vapor is discussed in multiple studies (Salminen 1988; Songok et al. 2014; Ma et al. 2022). Furthermore the pulp fibre wall has a large amount of nanoscale pores (Maloney and Paulapuro 1999). Those nanopores are enhancing the water take-up from the gas phase due to capillary condensation, which has e.g. been shown in paper drying studies

(Park et al. 2005). Because in sized paper, the contact angle is above 90°, which inhibits capillary flow, gas vapour flow is probably the most important contribution to water transport in sized papers.

These processes are inhomogeneous which leads to fibre areas with varying contact angle and therefore capillary forces. This will result in a finger like behaviour and explains the absence of a clear liquid front. Furthermore, liquid can start making bridges between regions separated by hydrophobised surfaces, a phenomenon called Haines jump (Berg et al. 2013; Sun and Santamarina 2019; O'Brien et al. 2020). These sudden jumps are accompanied by a quick fluid redistribution within the medium. At a certain point, the water reaches the bottom of the paper samples, making this area transparent as seen in Fig. 11.

In a final 3rd phase, water will fill the porous medium through areas that were prewetted. During this wetting period, water finds it easier to enter through regions that are already wet, initiating a rapid increase in moisture along these existing paths, as shown in Fig. 12. This was also verified by the growing transparent spots in Fig. 11. When the pore space is completely filled, the water will break the hydrogen bonds and allows the paper to start a second swelling process and reach its final thickness.



#### **Conclusions**

In this paper, liquid penetration experiments were conducted on papers with varying levels of calendering and hydrophobisation.

The first part of this study demonstrated that calendering decreased liquid front penetration speed, and the Gurley air permeance proved to be a good measure for the reduction in permeability. It could be concluded according to this convergence that calendering effects a topological compression of the matrix structure retaining the original nodal contact between fibres, such that the porosity decreases and the tortuosity in the depth direction increases. Furthermore, a guideline was presented for modelling liquid penetration in hydrophilic paper which indicated that for hydrophilic low-calendered paper, swelling could be neglected in penetration models. However, for highly calendered papers, swelling significantly influenced the penetration behaviour and cannot be neglected.

The second part of this study focused on the effect of hydrophobisation, which revealed that hydrophobisation delayed and slowed down liquid uptake in paper samples, and in extreme cases even completely changed the uptake behaviour. In highly hydrophobised papers, liquid penetration was governed prewetting of the fibres, most likely by liquid vapour transport. During this period a first swelling stage of the paper took place which was linked to an increase in fibre thickness. Both vapour transport and swelling decreased the hydrophobisation of the fibres, allowing water to fill the paper pore space. This, further increasing the paper thickness due to the breaking of hydrogen bonds between fibres.

By performing through-thickness moisture profiles during penetration, this paper could contribute to enhance our understanding of the complex penetration in paper and the effects of post processes such as calendering and hydrophobisation. A better understanding of these processes on the penetration characteristics will result in an improved control of the flow mechanisms, benefiting applications such as printing, microfluidics, cleaning papers and much more. Acknowledgements This publication is part of the project PQP (Print Quality and Particles) (Project No. 17099) of the research collaboration program High Tech Systemen en Materialen (HTSM) 2018 TTW, which was (partly) financed by the Dutch Research Council (NWO). The researchers would also like to thank H. Dalderop (TU/e) and M. Kurvers (TU/e) for helping to build the experimental setup. Last, we would like to thank Covestro and Canon Production Printing for their support.

**Author contributions** R.N. Conceptualization, Investigation, Writing, Data analysis, Writing - original draft C.W. Data analysis and sample preparation U.H.: Provided the paper samples and helped in analysing the data and shaping the story. S.E.: Supervision, Data analysis, Review and Editing, Project administration O.A.: Supervision, Review and Editing, Funding acquisition, Project administration U.H.: Supervision, Data analysis, Conceptualization, Review and Editing, Funding acquisition, Project administration

**Funding** This publication is part of the project PQP (Print Quality and Particles) (Project No. 17099) of the research collaboration program High Tech Systemen en Materialen (HTSM) 2018 TTW, which was (partly) financed by the Dutch Research Council (NWO).

**Data availability** The authors confirm that the data supporting the findings of this study are available within the article.

#### **Declarations**

**Competing interests** The authors declare no competing interests

**Ethical approval** No animal or human studies were carried out by the authors.

**Conflict of interest** This article does not involve any conflicts of interest.

#### Appendix 1 Calendered papers

In this appendix, extra information about the calendered papers is provided. Figure 13 provides the moisture profiles of the C15H00 and C30H00 papers. The profiles show similar behaviour to the C60H00 paper shown in Fig. 2. The calendered papers show more swelling and more deformation after liquid penetration compared to lightly calendered C00H00 paper.



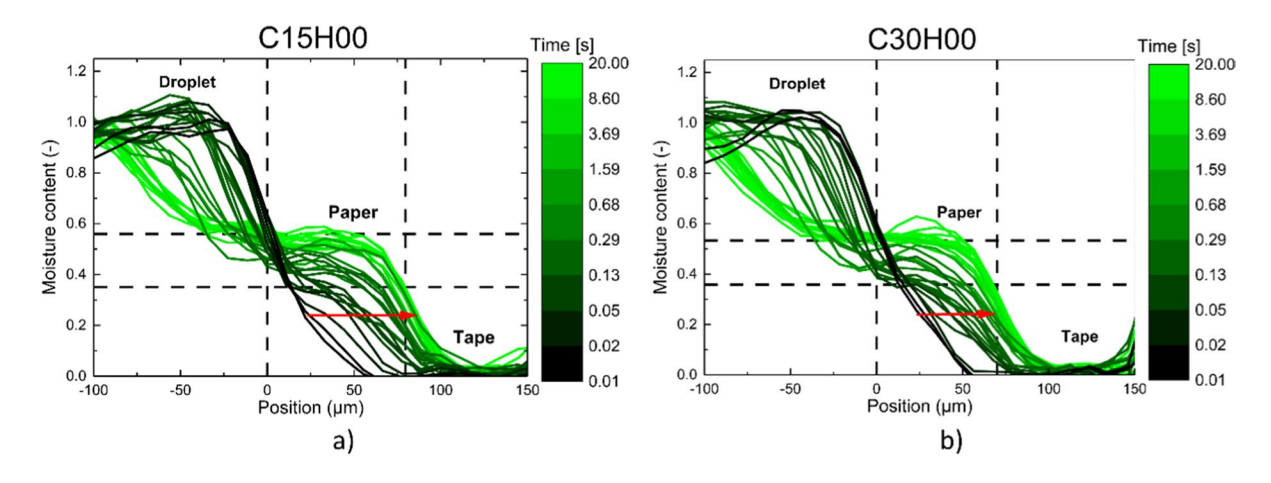
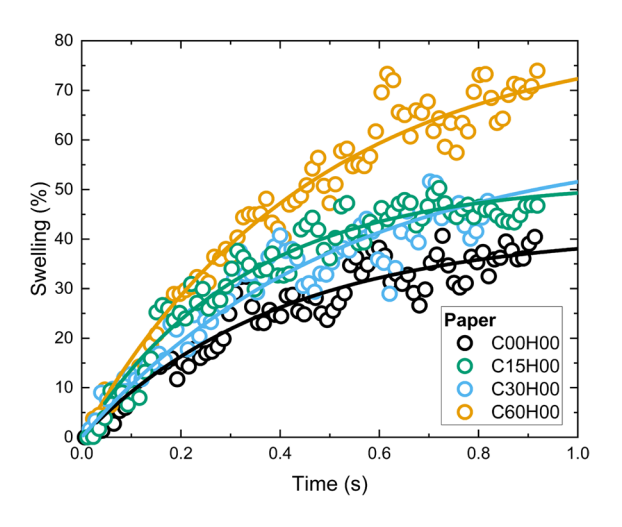


Fig. 13 Liquid profiles measured during the penetration of a Clariscan-water solution within a) C15H00 and b) C30H00 paper. A green scale is used to identify the time at which the profile is measured

Also for C15H00 and C30H00, the swelling curves are provided in Fig. 14. It can be seen that for larger differences in calendering forces (C00 and C60) a clear difference can be observed but that for C15H00 and C30H00 the swelling behaviour becomes quite comparable. The fitting parameters found for C15H00 and C30H00 are  $k = 3.03 \pm 0.12$ ,  $S_{\rm max} = 52 \pm 0.6$  and  $k = 1.92 \pm 0.12$ ,  $S_{\rm max} = 67 \pm 0.5$ , respectively.



**Fig. 14** Swelling as a function of time for C00H00 (black), C15H00 (green), C30H00 (blue) and C60H00 (orange). The lines corresponding to a fit based on a swelling model given by:  $S = S_{max}(1-e^{-kt})$ 

## Appendix 2 Hydrophobised papers

In this appendix, the moisture profiles for the C00H20 papers are provided for completeness, as shown in Fig. 15. The profiles show similar behaviour to the C00H10 paper shown in Fig. 7a.

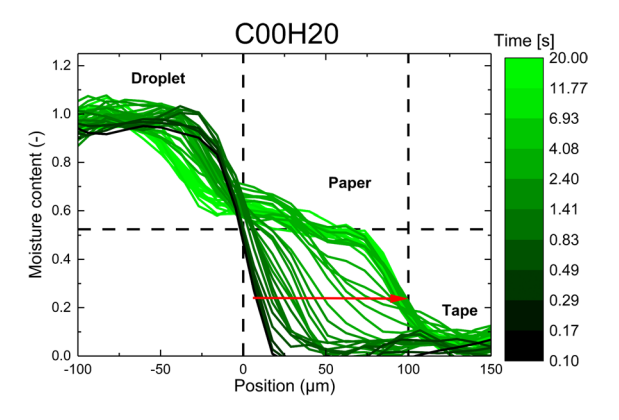


**Fig. 15** Liquid profiles measured during the penetration of a Clariscan-water solution within C00H20 paper. A green scale is used to identify the time at which the profile is measured



Open Access This article is licensed under a Creative Commons Attribution 4.0 International License, which permits use, sharing, adaptation, distribution and reproduction in any medium or format, as long as you give appropriate credit to the original author(s) and the source, provide a link to the Creative Commons licence, and indicate if changes were made. The images or other third party material in this article are included in the article's Creative Commons licence, unless indicated otherwise in a credit line to the material. If material is not included in the article's Creative Commons licence and your intended use is not permitted by statutory regulation or exceeds the permitted use, you will need to obtain permission directly from the copyright holder. To view a copy of this licence, visit <a href="https://creativecommons.org/licenses/by/4.0/">https://creativecommons.org/licenses/by/4.0/</a>.

#### References

- Akinli-Kogak, Sedef. 1997. "THE INFLUENCE OF FIBER SWELLING ON PAPER WETTING."
- Arends T, Pel L, Smeulders D (2018) Moisture Penetration in Oak during Sinusoidal Humidity Fluctuations Studied by NMR. Constr Build Mater 166(March):196–203. https://doi.org/10.1016/J.CONBUILDMAT.2018.01.133
- Babaremu K, Oladijo OP, Akinlabi E (2023) Biopolymers: A Suitable Replacement for Plastics in Product Packaging. Adv Indust Eng Polym Res 6(4):333–340. https://doi.org/10.1016/J.AIEPR.2023.01.001
- Benmessaoud N, Hamri S, Bouchaour T, Maschke U (2020) Swelling and Thermal Behavior of a Cross-Linked Polymer Networks Poly(2-Phenoxyethyl Acrylate): Exploitation by the Voigt Viscoelastic Model. Polym Bull 77(10):5567–5588. https://doi.org/10.1007/S00289-019-03040-2/TABLES/3
- Berg S, Ott H, Klapp SA, Schwing A, Neiteler R, Brussee N, Makurat A et al (2013) Real-Time 3D Imaging of Haines Jumps in Porous Media Flow. Proc Natl Acad Sci USA 110(10):3755–3759. https://doi.org/10.1073/PNAS.12213 73110
- Blanco A, González G, Casanova E, Pirela ME, Alexander Brice~no. (2013) Mathematical Modeling of Hydrogels Swelling Based on the Finite Element Method. Appl Math 2013(08):161–170. https://doi.org/10.4236/AM.2013.48A022
- Böhm A, Biesalski M (2017) Paper-Based Microfluidic Devices: A Complex Low-Cost Material in High-Tech Applications. MRS Bull 42(5):356–364. https://doi.org/ 10.1557/MRS.2017.92
- Browne T, Crotogino R (2018) "Future directions in calendering research". BioResources, 1001–36. https://doi.org/10.15376/FRC.2001.2.1001

- Chang S, Kim W (2020) Dynamics of Water Imbibition through Paper with Swelling. J Fluid Mech 892:A39. https://doi.org/10.1017/JFM.2020.219
- Darcy H (1856) Les Fontaines Publiques de La Ville de Dijon.

  Paris. https://books.google.com/books?hl=nl&lr=&id=yXKx1zPVQMUC&oi=fnd&pg=PA1&ots=UdPf6mFhb8&sig=OYnHQPq50qWNi9ngGCRFiLLMLrs
- Derraik JGB (2002) The Pollution of the Marine Environment by Plastic Debris: A Review Jos e e G. Mar Pollut Bull 44(9):842–852. https://doi.org/10.1016/S0025-326X(02) 00220-5
- Dziuba R, Kucharska M, Madej-Kiełbik L, Sulak K, Wiśniewska-Wrona M (2021) Biopolymers and Biomaterials for Special Applications within the Context of the Circular Economy. Materials 14(24):7704. https://doi.org/10.3390/MA14247704
- Gong MM, Sinton D (2017) Turning the Page: Advancing Paper-Based Microfluidics for Broad Diagnostic Application. Chem Rev 117(12):8447–8480. https://doi.org/10. 1021/ACS.CHEMREV.7B00024
- Hodgson KT, Berg JC (1988) The Effect of Surfactants on Wicking Flow in Fiber Networks. J Colloid Interface Sci 121(1):22–31. https://doi.org/10.1016/0021-9797(88) 90404-3
- Huinink H (2016). Fluids in Porous Media: Transport and Phase Changes. Fluids in Porous Media: Transport and Phase Changes. https://doi.org/10.1088/ 978-1-6817-4297-7.
- Ilyas M, Ahmad W, Khan H, Yousaf S, Khan K, Nazir S (2018) Plastic Waste as a Significant Threat to Environment -A Systematic Literature Review. Rev Environ Health 33(4):383–406. https://doi.org/10.1515/REVEH-2017-0035/ASSET/GRAPHIC/J\_REVEH-2017-0035\_FIG\_ 005\_JPG
- Kannangara D, Shen W (2008) Roughness Effects of Cellulose and Paper Substrates on Water Drop Impact and Recoil. Physicochem Eng Aspects 330:151–160. https://doi.org/ 10.1016/j.colsurfa.2008.07.056
- Korpela A, Jaiswal AK, Asikainen J (2021) Effects of Hydrophobic Sizing on Paper Dry and Wet-Strength Properties: A Comparative Study between AKD Sizing of NBSK Handsheets and Rosin Sizing of CTMP Handsheets. BioResources 16(3):5350–60. https://doi.org/10.15376/BIORES.16.3.5350-5360
- Kuijpers CJ, van Stiphout TAP, Huinink HP, Tomozeiu N, Erich SJF, Adan OCG (2018) Quantitative Measurements of Capillary Absorption in Thin Porous Media by the Automatic Scanning Absorptometer. Chem Eng Sci 178:70–81. https://doi.org/10.1016/j.ces.2017.12.024
- Li Y, He B (2011) Characterization of Ink Pigment Penetration and Distribution Related to Surface Topography of Paper Using Confocal Laser Scanning Microscopy. BioResources 6(3):2690–2702
- Li Xu, Tian J, Shen W (2010) Progress in Patterned Paper Sizing for Fabrication of Paper-Based Microfluidic Sensors.



- Cellulose 17(3):649–659. https://doi.org/10.1007/S10570-010-9401-2/FIGURES/8
- Lundberg A, Örtegren J, Alfthan E, Ström G (2011) Paper-Ink Interactions: Microscale Droplet Absorption into Paper for Inkjet Printing. Nord Pulp Pap Res J 26(1):142–150. https://doi.org/10.3183/NPPRJ-2011-26-01-P142-150
- Ma X, Maillet B, Brochard L, Pitois O, Sidi-Boulenouar R, Coussot P (2022) Vapor-Sorption Coupled Diffusion in Cellulose Fiber Pile Revealed by Magnetic Resonance Imaging. Phys Rev Appl 17(2):024048. https://doi.org/ 10.1103/PHYSREVAPPLIED.17.024048/FIGURES/11/ MEDIUM
- Maloney T, Paulapuro H (1999) "The Formation of Pores in the Cell Wall." Journal of Pulp and Paper Science 25 (12): 430. https://research.aalto.fi/en/publications/the-forma tion-of-pores-in-the-cell-wall.
- Masoodi R, Pillai KM (2010) Darcy's Law-Based Model for Wicking in Paper-like Swelling Porous Media. AIChE J 56(9):2257–2267. https://doi.org/10.1002/AIC.12163
- Modaressi H, Garnier G (2002) Mechanism of Wetting and Absorption of Water Droplets on Sized Paper: Effects of Chemical and Physical Heterogeneity. Langmuir 18(3):642–649. https://doi.org/10.1021/LA0104931/ASSET/IMAGES/MEDIUM/LA0104931E00012.GIF
- Murali V, Venditti G, Zeegers JCH, Darhuber AA (2021) Inkjet Deposition of Lines onto Thin Moving Porous Media -Experiments and Simulations. Int J Heat Mass Transf 176(September):121466. https://doi.org/10.1016/J.IJHEA TMASSTRANSFER.2021.121466
- Nicasy RJK, Huinink HP, Erich SJF, Adan OCG, Tomozeiu N (2023) Ultra Fast Imaging NMR Method for Measuring Fast Transport Processes in Thin Porous Media. Magn Reson Imaging 103(November):61–74. https://doi.org/10. 1016/j.mri.2023.06.009
- Nicasy RJK, Waldner C, Erich SJF, Adan OCG, Hirn U, Huinink HP (2024) Liquid Uptake in Porous Cellulose Sheets Studied with UFI-NMR: Penetration, Swelling and Air Displacement. Carbohyd Polym 326(February):121615. https://doi.org/10.1016/J.CARBPOL.2023. 121615
- O'Brien A, Afkhami S, Bussmann M (2020) Pore-Scale Direct Numerical Simulation of Haines Jumps in a Porous Media Model. Eur Phys J Special Top 229(10):1785–98. https:// doi.org/10.1140/EPJST/E2020-000008-0
- Oliver JF, Agbezuge L, Woodcock K (1994) A Diffusion Approach for Modelling Penetration of Aqueous Liquids into Paper. Colloids Surf, A 89(2–3):213–226. https://doi. org/10.1016/0927-7757(94)80120-7
- Park S, Venditti RA, Pawlak JJ, Jameel H (2005) "High resolution thermo-gravimetric analysis of pulp drying". Trans XIIIth Fund Res Symp. *Cambridge*, 161–86. https://doi.org/10.15376/frc.2005.1.161.

- Resch P, Hirn U, Bauer W (2010) Calendering Effects on Coating Pore Structure and Ink Setting Behavior. Tappi J 9(1):27–35
- Rida A, Yang Li, Vyas R, Tentzeris MM (2009) Conductive Inkjet-Printed Antennas on Flexible Low-Cost Paper-Based Substrates for RFID and WSN Applications. IEEE Antennas Propag Mag 51(3):13–23. https://doi.org/10. 1109/MAP.2009.5251188
- Saft S, Kaliske M (2013) A Hybrid Interface-Element for the Simulation of Moisture-Induced Cracks in Wood. Eng Fract Mech 102(April):32–50. https://doi.org/10.1016/J.ENGFRACMECH.2013.02.010
- Salminen P (1988) Studies of Water Transport in Paper during Short Contact Times. Ph.D Thesis. Abo Akademi University, Turku
- Samyn P (2013) Wetting and Hydrophobic Modification of Cellulose Surfaces for Paper Applications. J Mater Sci 48(19):6455–6498. https://doi.org/10.1007/S10853-013-7519-Y
- Seidlhofer T, Hirn U, Teichtmeister S, Ulz MH (2022) Hygro-Coupled Viscoelastic Viscoplastic Material Model of Paper. J Mech Phys Solids 160(March):104743. https:// doi.org/10.1016/J.JMPS.2021.104743
- Shallhorn P, Gurnagul N (2009) "A simple model of the air permeability of paper." Adv Pulp Paper Res, 475–90. https://doi.org/10.15376/frc.2009.1.475.
- Songok J, Toivakka M (2016) Controlling Capillary-Driven Surface Flow on a Paper-Based Microfluidic Channel. Microfluid Nanofluid 20(4):1–9. https://doi.org/10.1007/ S10404-016-1726-1/FIGURES/10
- Songok J, Salminen P, Toivakka M (2014) Temperature Effects on Dynamic Water Absorption into Paper. J Colloid Interface Sci 418(March):373–377. https://doi.org/10.1016/J. JCIS.2013.12.017
- Sun,Z, Santamarina Z (2019) "Haines Jumps: Pore Scale Mechanisms." Phys Rev E 100(2). https://doi.org/10.1103/ physreve.100.023115.
- Szlek DB, Reynolds AM, Hubbe MA (2022) Hydrophobic Molecular Treatments of Cellulose-Based or Other Polysaccharide Barrier Layers for Sustainable Food Packaging: A Review. BioResources 17(2):3551–3673. https:// doi.org/10.15376/BIORES.17.2.SZLEK
- Tang XZ, Kumar P, Alavi S, Sandeep KP (2012) Recent Advances in Biopolymers and Biopolymer-Based Nanocomposites for Food Packaging Materials. Crit Rev Food Sci Nutr 52(5):426–442. https://doi.org/10.1080/10408 398.2010.500508
- Tayeb AH, Tajvidi M, Bousfield D (2020) Paper-Based Oil Barrier Packaging Using Lignin-Containing Cellulose Nanofibrils. Molecules 25(6):1344. https://doi.org/10. 3390/MOLECULES25061344
- Thuppahige W, Thathsaranee V, Karim MA (2022) A Comprehensive Review on the Properties and Functionalities of Biodegradable and Semibiodegradable Food Packaging



5544 Cellulose (2024) 31:5527–5544

Materials. Compr Rev Food Sci Food Safe 21(1):689–718. https://doi.org/10.1111/1541-4337.12873

- Vallabh R, Ducoste J, Seyam AF, Banks-Lee P (2011) Modeling Tortuosity in Thin Fibrous Porous Media Using Computational Fluid Dynamics. J Porous Media 14(9):791–804. https://doi.org/10.1615/JPORMEDIA.V14.I9.40
- Vernhes P, Bloch JF, Blayo A, Pineaux B (2009) Effect of Calendering on Paper Surface Micro-Structure: A Multi-Scale Analysis. J Mater Process Technol 209(11):5204– 5210. https://doi.org/10.1016/j.jmatprotec.2009.03.005
- von Bahr M, Seppanen R, Tilberg F, Zhmud B (2004) Dynamic Wetting of AKD-Sized Papers. J Pul and Paper Sci 30(3):74–81
- Waldner C, Hirn U (2023) Modeling Liquid Penetration into Porous Materials Based on Substrate and Liquid Surface Energies. J Colloid Interf Sci 640(June):445–455. https:// doi.org/10.1016/J.JCIS.2023.02.116
- Waldner C, Mayrhofer A, Hirn U (2022) Measuring Liquid Penetration in Thin, Porous Sheets with Ultrasound and Drop Absorption – Scope and Limitations. Colloids Surf, A 650(October):129551. https://doi.org/10.1016/J. COLSURFA.2022.129551
- Waldner C, Ritzer A, Hirn U (2023) "Modeling Inkjet Dots from Drop Spreading, Absorption and Evaporation-An Engineering Approach." https://doi.org/10.1016/j.colsu rfa.2023.131986
- Wu N, Hubbe MA, Rojas OJ, Park S (2009) Permeation of Polyelectrolytes and Other Solutes into the Pore Spaces of Water-Swollen Cellulose: A Review. Bioresources 4(3):1222–62. https://doi.org/10.15376/BIORES.4.3.1222-1262
- Wulz P, Waldner C, Krainer S, Kontturi E, Hirn U, Spirk S (2021) Surface Hydrophobization of Pulp Fibers in Paper Sheets via Gas Phase Reactions. Int J Biol Macromol

- 180(June):80–87. https://doi.org/10.1016/J.IJBIOMAC. 2021.03.049
- Xie X, Samsudeen F, Farnood R, Kortschot MT, Spelt JK (2008) Roughening Due to Ink Jet Rewetting: Effect of Paper Treatment and Composition. J Imaging Sci 52(1):10506-1-1-105067
- Xu Y, Enomae T (2014) Paper Substrate Modification for Rapid Capillary Flow in Microfluidic Paper-Based Analytical Devices. RSC Adv 4(25):12867–12872. https://doi. org/10.1039/C4RA00434E
- Xu J, Liu F, Tao Wang H, Goff D, Zhong F (2020) Fabrication of Films with Tailored Properties by Regulating the Swelling of Collagen Fiber through PH Adjustment. Food Hydrocolloids 108(November):106016. https://doi.org/10.1016/j.foodhyd.2020.106016
- Yavari N, Azizian S (2022) "Mixed Diffusion and Relaxation Kinetics Model for Hydrogels Swelling" https://doi.org/ 10.1016/j.molliq.2022.119861
- Zhang K, Feng W, Jin C (2020) Protocol Efficiently Measuring the Swelling Rate of Hydrogels. MethodsX 7(January):100779. https://doi.org/10.1016/J.MEX.2019.100779

**Publisher's Note** Springer Nature remains neutral with regard to jurisdictional claims in published maps and institutional affiliations.

